Available online at www.sciencedirect.com
ScienceDirect
Catalysis Today 130 (2008) 527–536
CATALYSIS TODAY
www.elsevier.com/locate/cattod

Conversion of propylene into cyclohexane on PtGaZr/SiO_2 catalyst

Roberto Galiasso Tailleur *, Jose Bonilla Platin

Simon Bolivar University, Department of Thermodynamics, Sartenejas, Baruta, Venezuela

Available online 26 November 2007

Abstract

The light olefins present in Delay Coker and fluid catalytic cracker dry gas can be valorized into naphthenes using a new PtGaZr/SiO_2 catalyst. This catalyst was compared to a $GaZrSiO_2$ catalyst prepared with the same methodology. Both were characterized by XRD, and FTIR, XPS, ^{71}Ga, ^{29}Si and ^{1}H NMR spectroscopies. Propylene is treated in the presence of CS_2, hydrogen, and benzene in a semi-batch type reactor and the product composition is analyzed by GC and MS techniques. The different operating variables were explored to study the effect of Pt on activity, selectivity and catalyst stability. The spent catalysts after 10 cycles in operation were analyzed using ^{13}C NMR, ^{1}H NMR, IR, and XPS spectroscopies. The paper discusses the catalytic surface composition, the effect of temperature, contact time, hydrogen partial pressure and benzene in the feed. The study demonstrated that the effect of Pt, hydrogen and benzene is crucial to orient the reaction toward naphthenes production.
© 2007 Elsevier B.V. All rights reserved.

Keywords: Propylene; Dimerization; PtGaZr/SiO_2 catalyst; Kinetics; Aromatics; Cycloparaffins

1. Introduction

The light olefins produced from fluid catalytic crackers and coking units have traditionally been considered low-value by-products and used as fuel gas. It is hard to improve their valorization due to their low olefins content, and to the presence of diolefins and sulfur that deactivate the traditional catalysts used for polymerization [1,2]. By employing the adequate purification method, however alkylates and oxygenates can be produced to yield high-value gasoline blending components or petrochemical products. Another useful alternative is the oligomerization of olefins and paraffins into aromatics and cycloalkanes as it was proposed by several authors [3–5]. Most of the heterogeneous dimerization–oligomerization technology depends on catalyst stability due to the tendency of zeolites to produce coke [6,7]. MFI-type Ga-ZSM-5 has been reported to have excellent activity in aromatization of propane and butane [8,9] to produce aromatics. Ga on mesoporous SiO_2 base materials gave the possibility of a selective conversion into bulky type molecules, with low diffusion control and with particular shape-oriented reactions in the zeolite cages [10,11]. The simultaneous conversion of propylene and propane into benzene is one of the options, but still limited by the catalyst deactivation. The role of acidity in coke formation remains a critical issue. Studies were carried out with propylene and Ga/FMI type zeolites [12–15], among others. In spite of that few improvements have been made in catalyst stability. We had introduced a new type of solid base on PtGaZr/MCM-41 [5], and more recently a PtGaZr/SiO_2 type catalyst [16]. The idea is to control the deactivation and the type of acid sites present in surface and stabilize them by a hydrothermal treatment. We have tried to develop a surface structure where the Pt nanodispersed plays a role, other than doing the classical hydrogenation–dehydrogenation reactions, in the acid sites build up. The formation of carbonaceous insoluble material on the catalyst seems to be promoted by strong acid sites via polymerization, dehydrogenation, and aromatization reactions of the olefins. This deposit might block other surrounding acid sites and the mouth of the pores, thereby reducing the access and the number of active site. Galiasso and Platin [5] demonstrated that the presence of partial pressure of hydrogen and the use of benzene as solvent have a favorable effect on catalyst life.

This work focuses on studying the effect of Pt on catalyst activity, selectivity and stability for propylene conversion into cyclohexane using a new catalyst base on PtGaZr/SiO_2. The experimental part compares the performance of the catalyst

* Corresponding author. Current address: Chemical Engineering Department, TA&M University, College Station, TX 77843, United States.
E-mail address: reg2005@chemail.tamu.edu (R.G. Tailleur).

0920-5861/$ – see front matter © 2007 Elsevier B.V. All rights reserved.
doi:10.1016/j.cattod.2007.10.073

prepared with and without Pt via cogelation and steam treatment for the conversion of propylene.

2. Experimental

2.1. Catalyst preparation

The catalyst was prepared in Teflon-lined autoclave using a modified method from that of Wu et al. [17], who synthesized SBA-15. A quantity of 6 g of Pluronic 123 (Aldrich-5800 average molecular weight) was dissolved in 200 g of a 2 M hydrochloric acid. Then 9.25 g of tetraethyl orthosilicate (TEOS, Fluka) was added under intense stirring and kept at room temperature for 6 h; then 5 g of gallium nitrate (Aldrich, 99%) and 12 g of zirconium sulfate (Aldrich 98%) were added under intense stirring and kept for 2 h at room temperature. After that the reactor was heated to 375 K and maintained at this temperature without agitation for 24 h; and then cooled to room temperature. An aqueous solution of ammonium hydroxide (20%) was added to obtain a neutral pH. The solution was reheated again to 373 K, kept for another 24 h without agitation, and cooled back to room temperature. The final solid was then filtered, washed with several portion of ammonium hydroxide, dried under nitrogen for 4 h at 393 K, and calcinated in air at 673 K. This solid is mentioned on the paper ''as synthesize''. After that the solid was placed in a tubular reactor and treated in presence of steam and ammonium stream, at 473 K for 3 h to obtain the Ga and Zr migration out of the framework; then the solid was calcinated in air to 773 K for 8 h. This procedure is called hydrothermal treatment and the resulting solid mentioned as GaZr. The latter was impregnated with an aqueous solution of Pt diamine-chloride compound (Aldrich, 98%) at room temperature, and subsequently washed, filtered, dried in air at 330 K for 3 h, and calcinated in air at 673 K for another 3 h. The catalyst is called PtGaZr. Both solids were activated under hydrogen, spiked with 50 ppm of CS_2, at 450K for 2 h and called fresh (F) catalyst. After reaction the spent catalyst (S) is obtained.

2.2. Catalysts characterization

GaZr(F) and PtGaZr(F) catalysts were characterized. They operated during 10 cycles at the same conditions but in each cycle a new feed was reintroduced keeping the same catalyst. At the end of the 10 cycles the spent (S) samples were obtained.

2.2.1. Pore structure

Nitrogen sorption experiments and BET or BJH analysis were used to characterize the pore structure. The measures were performed in a Micromeritics ASAP 2010 apparatus at 70 K. Adsorption–desorption measurements were automatically performed with 5 s equilibration time for each point. The software calculated the pore size distribution in the microregion and the average pore radius in the mesoporous region.

2.2.2. Effective diffusivity

The fresh and used catalysts in 2–5 μm powder diameter were compressed (10 Tn/mm^2) to obtain cylinders of 1 mm diameter and 8 mm length. Then each catalyst was installed in a shallow-bed string reactor [18] where a pulse of benzene in argon was passed parallel to the external surface and the effective diffusivity measured at 80 °C, 0.1 MPa of pressure. The inert gas helium was flowed at 2 cm^3/s until the pressure and temperature in the system were constant. The detector measuring the inlet and outlet concentration was calibrated to have a linear response at the concentration of pentane selected for the test. Then, a pulse of benzene was injected in the chamber and the concentration at the inlet and outlet of the cells that contain the fresh or the spent catalysts were measured to determine their macro- and mesoporous effective diffusivity using a technique developed in the 1990 by the author [18]. The meso-diffusivity associated to the initial powder of catalyst is reported in Table 1.

2.2.3. X-ray diffraction

X-ray powder diffraction has been performed in a Philips PW-1830 diffractometer equipped with a graphite monochromator. The data was obtained with 0.02° step size, using 3 s in each step, and the spectra were analyzed using commercial software in the range of 0–10° (2θ).

2.2.4. Chemical analysis

The concentration of C, S, Zr, Ga, and Pt were determined by AAS.

2.2.5. Acidity (TGA-FTIR)

The IR spectroscopy of the catalyst on KBr was carried out using a Perkin-Elmer FTIR with DGS. The regions from 1600 to 1000 cm^{-1} and from 3600 to 3000 cm^{-1} were analyzed before and after adsorption of pyridine. The catalyst samples were treated in a specially designed reaction cell. There, they were degassed in vacuum at 1 Torr for 20 min, and then

Table 1
Set of reactions for propylene[a]

	HC	H_2	Main products	
C_3H_6	C_3H_6	–	→MeCP	$CH_3C_5H_9$
C_3H_6	–	1	→Propane	C_3H_8
$CH_3C_5H_9$	–	–	→CH	C_6H_{12}
$CH_3C_5H_9$	C_3H_6	–	→DMeCP	$(CH_3)_2C_5H_8$
$(CH_3)_2C_5H_8$	C_3H_6	–	→TMeCP	$(CH_3)_3C_5H_7$
C_3H_6	C_3H_6	–	→*n*-OC_6	C_6H_{12}
C_6H_{12}	C_3H_6	–	→*n*-OC_9	C_9H_{18}
C_6H_{12}	–	1	$\rightarrow C_2 + iC_4^=$	$C_2H_6 + C_4H_8$
C_9H_{18}	–	1	$iC_4 + nOC_5$	$C_4H_{10} + C_5H_{10}$
C_4H_8	C_3H_6	–	→DMCP	$(CH_3)_2C_5H_8$
C_5H_{10}	C_3H_6	–	→TMCP	$(CH_3)_3C_5H_7$
$(CH_3)_2C_5H_8$	–	–	→MCH	$CH_3C_6H_{11}$
C_4H_8	C_3H_6	–	→*n*-OC_7	C_7H_{14}
C_5H_{10}	C_3H_6	–	→*n*-OC_9	C_8H_{16}
C_nH_n		1	↔	$C_nH_n + 2$
C_6H_{12}	–	±3	↔B	C_6H_6

[a] Similar reactions may occurred with other olefins.

contacted at room temperature with a stream of argon (5 cm^3/min) containing 0.1% pyridine. After that, the cell was heated at 373 °C and 393 K in argon to desorb the pyridine. The values were reported as micromole of pyridine per g of sample.

2.2.6. ^{71}Ga NMR, ^{29}Si NMR, ^{13}C NMR and ^{1}H NMR analysis

The ^{71}Ga NMR spectra were obtained with a Bruker AMX-300 operating at 228 MHz. The sample was spun up to 10 kHz with air using 5-μs pulse in a 50 ms recycle delay and 200,000 scans. GaO was used as standard internal. ^{29}Si NMR was measured operating at 79.49 MHz with a pulse of 5-μs duration, with a MAS probe of 3 mm, using 10,000 scans. ^{13}C NMR analyses of the carbon deposits on solids were performed operating at frequency of 75.4 MHz with cross-polarization, magic angle spinning (CP/MAS) and DD techniques using a rotor speed of 4.8 MHz. A total of 10,000 acquisitions were accumulated using a pulse width of 5-μs, a repetition delay 1 s and a contact time of 1 ms. The technique allowed us to detect the type of carbon present on surface using TMS as primary reference and hexamethylbenzene as secondary reference. ^{1}H NMR hydroxyls spectra were obtained at 400.1 MHz, with the same spectrometer, with a 2 nm MAS probe and a sample spinning rate of 8 MHz and 500 scans. TMS and HFP (hexafluor-propanol) were used as reference.

2.2.7. X-ray-photoelectron-spectroscopy

The spectra were obtained in a Bruker 300 apparatus (Mg cathode) using a power of 50 eV (Ref C_{1s}: 285.0 eV). XPS analyses employed to assess the metal dispersion on catalysts using the peak area intensity (corrected) to measure atomic concentration. Binding energies were measured in fresh oxide catalysts. The Shirley-type background was subtracted and the Zr, Ga, Si, and O species were measured by peaks deconvolution and integration to obtain the area [19]. The signals are reported here as a ratio: intensities of the metal respect to the sum of intensities of all the metal present on surface. Pt at the low concentration used here, was feebly detected.

2.3. Chemical reactions

The effects of the operating variables were obtained in a small-scale semi-batch (pseudo-isothermal) type of reactor. This unit has a volume of 30 cm^3, operated at different temperature, 1.0 MPa of total pressure and 300 rpm of stirring rate. At the beginning 1 g of catalyst together with 15 g of benzene (solvent) were introduced in the reactor, sealed and pressurized to 0.5 MPa by a stream containing 5 mol of hydrogen and 1 mol of propylene, spiked with 50 ppm of CS_2. The reactor was then heated to the reaction temperature and the pressure adjusted to 1.0 MPa using the same gas stream (hydrogen plus propylene spiked with 50 ppm of CS2). Then, the first sample of liquid was analyzed to determine the start of run concentrations. During the cycle, hydrogen was added continuously to maintain constant total pressure using an automatic pressure controller valve. In each cycle fives samples of liquid as a function of contact time were taken and analyzed using a Varian Gas Chromatograph (equipped with CP-Sil capillary column). The column activity was verified using a standard sample. Conversions of propylene and product distribution were calculated. After 0.4 h of contact time the reactor was cooled to room temperature, depressurized under small flow of hydrogen, and the liquid was withdrawn from the reactor. Then, a new charge of benzene, hydrogen, and propylene was added until obtaining again the 1 MPa of pressure. In this manner we proceed further to achieve ten cycles of operation (heating, pressure adjustment, liquid sampling) with the same catalyst. The test was duplicated. After reaction, the catalyst was separated by filtration, washed with xylene for 10 h at 263 K, dried in nitrogen, and kept sealed under nitrogen atmosphere for characterization. All tests used the same benzene/propylene ratio and three temperatures were explored (400, 410, and 420 K)

2.4. Set of reactions considered

The cyclization paths of reaction proceed through a first stage in which the olefins are adsorbed on an ''acidic'' type center. The adsorbed species suffer electronic delocalization to produce a carbocation that reacts with nearby adsorbed olefins to generate C_5, and C_6 cycloolefins, *n*- and *iso*-C_6 olefins that can be isomerized in place or desorbed. Bronsted and Lewis type center of medium-high strength is required for this reaction. When desorbed it can be cracked (β-scission) in a strong acid site to produce lower carbon number alkenes and another carbocation ion (lighter products). The olefins that desorbs (cyclic, or dimeric, or alkyl-cyclic) might migrate to the metal sites where they may be hydrogenated and hydrogenolyzed. Hydrogenation of linear olefins and cycloolefins could be fast enough on Pt as to be unable to control the global rate of reaction. This may not be the case on GaZr where the hydrogen transfer rate is slow. Only traces of diolefins and products higher than C_9 carbon number were found. For example, Table 1 shows the set of reactions considered for propylene.

2.5. Mass transfer control of the reactions

The mass transfer control for the faster reaction have been verified for the transport from the liquid to the film (k_{l-f}), and from the film to the solid (k_{f-s}) using the information experimentally measured by Tekie et al. [20] in a similar system. For example the rate of reaction for the propylene dimerization is calculated taking into account mass transfer of propylene

$$N_1 = k_{Li}A(C_{LP} - C_{SP}) = \eta_1 k_2' C_{SP}^2 a\mathrm{Fc} \quad (1)$$

For the hydrogenation the rate of reaction is calculated taken in account the mass transfer of propylene and hydrogen

$$N_2 = k_{LP}A(C_{LP} - C_{SP}) = \eta_2 k_2' C_{SP}^1 C_{SH_2} a\mathrm{Fc} \quad (2)$$

$$N_2 = k_{LH_2}A(C_{LH_2} - C_{SH_2}) = \eta_2 k_2' C_{SP} C_{SH_2} a\mathrm{Fc} \quad (3)$$

$$C_{SP} = \frac{k_{Li}AC_{LP}}{\eta_1 k_1' C_{SP} a\mathrm{Fc} + k_{LP}A} \quad (4)$$

$$C_{SP} = \frac{k_{LP} A C_{LP}}{\eta_2 k'_2 C_{SiH_2} a\mathrm{Fc} + k_{LP} A} \quad (5)$$

$$C_{SH_2} = \frac{k_{LSH_2} A C_{LH_2}}{\eta_2 k_2 C_{SP} a\mathrm{Fc} + k_{LH_2} A} \quad (6)$$

and then:

$$\gamma_1 = \eta_1 k_1 a\mathrm{Fc}\left(\frac{k_L A C_{LP}}{\eta_1 k'_{1j} C_{SP} aF + k_{LP} A}\right)^2 = \eta'_1 \eta_1 k'_{1j} C_{LP}^2 a\mathrm{Fc} \quad (7)$$

$$\gamma_2 = \eta_2 k_2 a\mathrm{Fc} \frac{k_{LP} A C_{LP}}{\eta_2 k'_{2j} C_{SH_2} aF + k_{LP} A} \frac{k_{LH_2} A C_{LH_2}}{\eta_2 k_2 C_{SP} a\mathrm{Fc} + k_{LH_2} A} = \eta'_2 \eta_2 k'_{2j} C_{LH_2} C_{LP} a\mathrm{Fc} \quad (8)$$

where D_{i7} is the molecular effective diffusivity (cm^2/s) of propylene in benzene; A is the area of one sphere (cm^2/cm^3), a is the activity coefficient and Fc factor that takes in account the mass of solid respect to 8 g used in the standard condition in the reaction. η' and η are the external and internal efficiency factor. For example, the mass transfer coefficient of propylene in benzene is $k_{l-f}A$: 0.00001 (1/s), and those of the benzene to the mesoporous silica $k_{f-s}A$: 0.0000017 (1/s). In addition the effective diffusivity in pores of propylene is $D_{eff} = 3.4 \times 10^9$ m^2/s and for hydrogen is $D_{eff} = 1.2 \times 10^8$ m/s, which were determined using the experimental values at different level of conversion and particle diameter.

3. Results and discussion

Let us start describing the catalyst properties, in particular the type of acid sites and metal dispersion on surface with and without Pt in a novel PtGaZr catalyst. Then we will proceed to discuss the activity, selectivity and stability at different operating conditions and analyze the role of Pt in presence of hydrogen and benzene. Finally we will interpret the mechanism of reaction using a simplified model for the path of reactions.

3.1. Catalysts physical properties

The two fresh catalysts had a similar a surface area (189 m^2/g), pore volume (0.48 cm^3/g), and a particle size of 1–4 μm obtained directly by synthesis. Notice that the method used during the initial part of the solid preparation is similar to that employed to prepare SBA-15 [17], but then the hydrothermal treatment modified the characteristic of the solids. The typical adsorption–desorption hysteresis loop generally observed for the SBA-15 type structure had mainly disappeared and both curves are quasi similar in fresh catalysts. They show a small micropore volume (0.1 cm^3/g), and a relative small contribution of micropore in the average pore diameter (8 nm). The coke deposition during the reaction produces a shift of the adsorption–desorption curves to lower pressure. The shape of the hysteresis curve is similar to those observed in fresh samples, indicating that the ratio pore-throat to pore-body diameter stays the same as coke is deposited in the pores. This implies that although pore narrowing occurred, the pore-mouth plugging seems to be avoided. There is a decrease in micropore volume and surface area of both PtGaZr(S) and GaZr(S) catalysts. Data given in Table 2 indicates about a 20 and 35% decrease in micropore volume, and 30 and 60% decreases in surface area, respectively. This can be ascribed to the formation of coke in the spent catalyst. The pore size distributions of fresh and coked catalysts shows a shift to a bigger average pore diameter in the catalyst sample without Pt and with high coke content, than in those with Pt, and a medium amount of coke content (Table 3). By the contrary, the effective diffusivity was slightly less decreased by the coke content in the pores of GaZr(S) than in PtGaZr(S) samples. This relative modification in diffusivity is associated to the access of C_5 molecules into a larger micro internal structure through pores of smaller diameter in PtGaZr(S) than in GaZr(S) catalyst.

Table 2
Catalyst properties before (F) and after (S) reaction

Catalyst	PtGaZr(F)	GaZr(F)	PtGaZr(S)	GaZr(S)
Number of cycles	0	0	10	10
Surface (m^2/g)	186	189	132	80
Pore volume (cm^3/g)	0.47	0.48	0.34	0.31
Micropore volume (cm^3/g)	0.12	0.14	0.096	0.081
Average pore A	80	81	75	77
D_{effMic} (cm^2/s) × 10^4	0.32	0.31	0.10	0.14

3.2. Catalyst bulk composition

The catalyst has a SiO_2/GaO ratio of 20 and a SiO_2/ZrO_2 of 30 wt% (see Table 3). The PtGaZr(F) samples contain lower amounts of Pt than any commercial reforming or isomerization catalysts. Fresh catalyst does not contain carbon, while spent ones shows the accumulation of coke as a function of the successive number of cycles in operation. As mentioned above, carbon accumulation is higher in the sample without Pt; this difference is attributed directly to the metal control of the amount of precursor via hydrogenation and indirectly via the effect of Pt in changing the acid type distribution, as it will be shown later. The difference observed in the sulfur content may be important. Sulfur was added on purpose to control the hydrogenolysis of the platinum and because the commercial feed contains sulfur. The effect (if any) of the sulfur in modifying the catalyst acidity is unknown.

Table 3
Chemical properties of the catalysts

	Catalyst			
	PtGaZr(F)	GaZr(F)	PtGaZr(S)	GaZr(S)
Pt (wt%)	0.1	–	0.1	–
ZrO_2/SiO_2 (wt%)	5			
GaO/SiO_2 (wt%)	3.33			
Carbon (wt%)	0	0	1.23	3.44
CS_2 insol. (wt%)	0	0	1.1	2.84
Sulfur % (wt%)	0.02	0.01	0.03	0.02

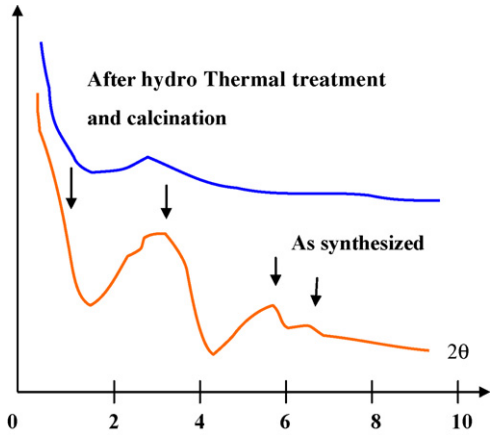

Fig. 1. XRD before and after hydrothermal and calcination treatment.

The XRD analysis of the sample before hydrothermal treatment shows three poorly defined peaks similar to those reported by Takeguchi [21], which are assigned to a regular Ga^{3+} distribution in a tetrahedral rod structure that grew around the surfactant in large gallium dispersion (Fig. 1). Another poorly defined signal that appears at 1° is attributed to SiO_2 (currently in SBA-15 structure) in the low-angle region. There is no signal in the range of 10–30°. These factors indicated an important degree of amorphization in the structure promoted by Zr octahedral intercalation in the framework. This amorphization increased during the hydrothermal treatment and it is responsible for the disappearance of all crystalline DRX signal, the loss in surface area, and the pore diameter broadening in the catalyst. No defined signal associated with cubic or monoclinic ZrO_2 or Ga_2O_3 species were detected, but the small bell shape in the background at 23° is associated to the increases of the unit cell by the Zr and Ga intercalated species in the framework.

The ^{71}Ga NMR spectra of the PtGaZr and GaZr samples were recorded with a large numbers of scans (Fig. 2). The as-synthesized sample presents two peaks at 7 and 150 ppm attributed to octahedral Ga^{3+} in Ga_2O_3 and a tetrahedral Ga^{3+} in siliceous environment in the framework. Similar peaks have been reported by Cheng et al. [22]. The hydrothermal treatment produce an important reduction in the 7 ppm signal and the

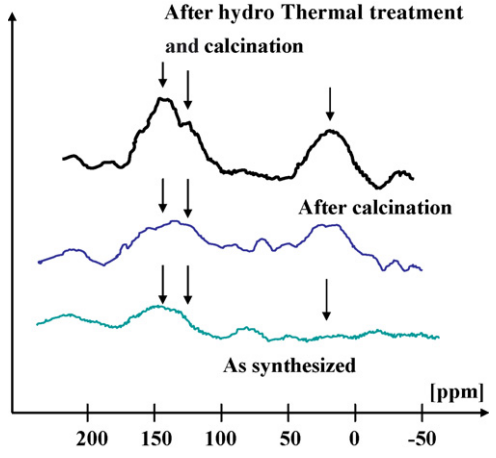

Fig. 2. ^{71}Ga NMR before and after hydrothermal and calcination treatment.

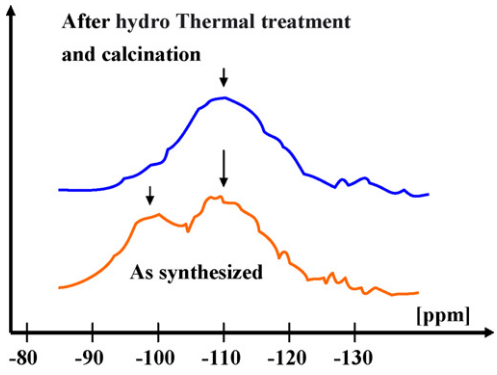

Fig. 3. ^{29}Si NMR before and after calcinations.

appearance of a new one at 175 ppm, assigned to $Ga^{3+}O_4$ of the Ga_2O_3 out-of-framework, similar to those observed on Ga-FMI [11].

The ^{29}Si NMR spectra shows a shifts to higher field (5 pm) in the Si (1 M) and Si (2 M) signal due to the hydrothermal treatment which produce a progressive elimination of Ga tetrahedral, and might be to a reduction on the Zr octahedral content in the framework. Fig. 3 shows the Q3 signal (−104 ppm) that is characteristic of the modification on the Si–O–Si environment by inclusion of some Ga in the framework; this signal disappear little by little when Ga migrated onto the surface. There is strong indication of the effect of Zr on the stabilization of the Ga in the framework and on surface, because after calcination at 700 or 800 K, both samples show no additional modification in the ^{27}Ga and ^{29}Si NMR signals. Pt may affect the Ga and Zr in the framework because, even when the Pt is incorporated on the surface of the GaZr solid via impregnation and posterior calcination, this thermal treatment provided an opportunity for the framework to be reorganized, factor well established in the specialized literature.

3.3. Catalysts surface composition

With the goal of determining the chemical species that may participate in the reaction, the PtGaZr(F) and GaZr(F) were evaluated by XPS (Table 4). The second column shows the binding energy and the third and fourth the ratio of the peak intensity for the Ga and Zr signal with respect to the intensity of Si, before (Be) and after (Af) hydrothermal treatment. The analysis of the PtGaZr(F) indicates a higher concentration of Ga^{3+} tetrahedric on surface after hydrothermal treatment than those observed in the as synthesized sample; this occurs because the Ga migrated from the framework onto the surface (Ga $3d_{5/2}$ varies from 0.4 to 1.3). That migration occurred with a small shift in the Ga signal from 21.6 toward 21.9 eV, and with some signal broadening, which is attributed to the Ga bridging a Zr species. This sample also has week signals (broad shoulder) at 20.2 eV due to the presence of Gallium oxide. The Zr XPS signal also increased in 0.2 eV and broadened after hydrothermal treatment. The observed oxygen signal (O 1 s, 533.2 eV) is enlarged after the hydrothermal treatment, and in addition a new signal appeared at 531.1 eV assigned to the oxygen bridge between Ga

Table 4
XPS analysis (before/after steam and calcination treatment)

Metal I_{Me}/I_{SiO_2}	Binding energy (eV)	PtGaZr(F) Be/Af (%)	GaZr(F) Be/Af (%)	PtGaZr(S) Af%	GaZr(S) Af%
Ga	21.5–21.8 $3d_{5/2}$	0.4/1.3	0.5/1.1	1.15	0.88
Zr	182.0–182.3 $3p_{3/2}$	2.2/3.4	2.2/2.4	3.25	2.1
Si	103.4 2p	–	–	–	–
C	284.4 2d	–	–	∼1.8	∼2.1

and Zr. It is important to note the presence of S2p species (102.8 eV) on surface, probably due to sulfur bonded to Pt clusters, which cannot be measured at this low level of concentration (Pt_{4f}: 72.2 eV) and high metal dispersion.

The same analysis performed on GaZr catalyst shows a small Ga^{3+} migration onto the surface (I_{Me}/I_{Si}: goes from 0.5 on as-synthesized to 1.1 in the fresh sample), a high amount of the Ga oxide and the absence of Ga^0 signal. The ratio of metal intensities indicated a lower dispersion than those measured in PtGaZr(F) catalyst. The same happened with Zr migration. Clearly the Pt may play a role on the Ga and Zr migration, dispersion and stabilization on surface. Diaz *et al*. [23] reported that by increasing the Pt content the presence of extra-framework Ga species increases in Ga/ZSM-5 system. These authors postulate that there is an inclusion of Pt in Ga structure on surface. In our case, the presence of Pt also modified the Zr, all of that is affecting the Ga dispersion as well as the type of compound formed between the tetragonally oriented Ga and the octahedrically oriented Zr oxides; thus we cannot distinguish the role of Pt on these two synergies. A preliminary CO adsorption study indicates a shift in the CO-Pt IR bands (from 3800 to 3830 cm^{-1}) and that Pt is well dispersed in the surface in a sort of solid solution.

The FTIR spectra of the PtGaZr(F) catalyst, before pyridine adsorption, presents a broad band in the zones of 960 and 3742 cm^{-1} (stretching bands) [24] similar than those of silanol groups on pure SBA-15. The spectra shows another band at 750 cm^{-1} that is attributed to Zr–O vibrations. The sample, after hydrothermal treatment, presents an increase in the 960 cm^{-1} IR bands, similar to those observed in Ti-SBA-15 thermal treatment [25]. In addition the catalyst has lost some intensity in the 3742 cm^{-1} band (after treatment the ratio I_{960}/I_{3742} goes from 0.4 to 0.7). The GaZr(F) shows similar IR bands but with different intensities. In addition the two catalysts present broad bands in the 230 nm region (UV–vis spectra) that are assigned to Zr (IV) in octagonal coordination [26] and they increase with the hydrothermal treatment.

The ^1H NMR analysis of the PtGaZr(F) hydroxyls are strongly affected by the Pt attenuation, but those of the GaZr(F) shows the presence of one small peak at 1.7 ppm attributed to the silanol group of the mesoporous silica, and a big shoulder between 4 and 6 ppm assigned to Bronsted-type hydroxyls (bridging OH). A similar signal was reported by Fang et al. [24] for Ga/MCM-41and assigned to the Ga-silanol groups on Si environment. Both signals were reduced by coking the catalyst.

3.4. Pyridine adsorption

The catalysts surface contains various types of acid sites that may adsorb pyridine: two are of the well known Bronsted-type attributed to the –OGa–OH–SiO– hydroxyls on surface, and the other to the –OGa–OH–ZrO– hydroxyls. Then there are two Lewis sites attributed to the same interactions (–OGa–O–SiO– and –OGa–O–ZrO–) in other coordination environment. Both, Bronsted and Lewis would provide a broader distribution of acid strengths. The FTIR (not shown) of the adsorbed pyridine molecule presents the typical bands of Ga–Si 1620, 1544, and 1456 cm^{-1}, and those of Ga–Zr at 1624, 1540 and 1460 cm^{-1} [27]. The 1620–1624 bands are attributed to pyridine coordinated in Ga^{3+} Lewis. Those bands at 1540–1544 are due to Bronsted acid sites. The catalyst also presents small bands at 1550, 1500 and 1680 cm^{-1} that are similar to those reported for Al-SBA-15, indicating a more complex pattern of Ga interactions with the surface of the zeolite than those observed by Gabelica et al. on Ga/AlZSM-5 [28].

Table 5 depicts the amount of pyridine that remains adsorbed at 473 and 573 K in the Bronsted type site (1540–44 cm^{-1}) and in the Lewis-type site (1440–1460 cm^{-1}) on calcinated catalyst. It can be seen that PtGaZr(F) presents at 473 and 573 K a lower Bronsted and a higher Lewis acidity than GaZr(F). This might be attributed to the effect of the Pt on Ga and Zr dispersion that favor the dehydroxylation of the acid site. The comparison of the IR signal due to isolated silanol groups at 3745 and 977 cm^{-1} confirm the lower OH content in Pt content catalyst.

The differences in acid sites and metal dispersion between the two catalysts must be taken in account to understand the activity, selectivity, and stability of them that follows.

3.5. Activity: effect of contact time and temperature

The catalysts were tested at a constant ratio of benzene to propylene, but changing the contact time, the temperature, and the hydrogen partial pressure. Fig. 4 shows –as an example– the

Table 5
Pyridine adsorption (FTIR) Bronsted/Lewis

Temperature (K)	PtGaZr(F) B/L	GaZr(F) B/L	PtGaZr(S) B/L	GaZr(S) B/L
473	0.4/1.2	0.5/0.8	0.2/0.8	0.1/04
573	0.1/0.9	0.05/0.7	0.05/0.45	0.05/0.2

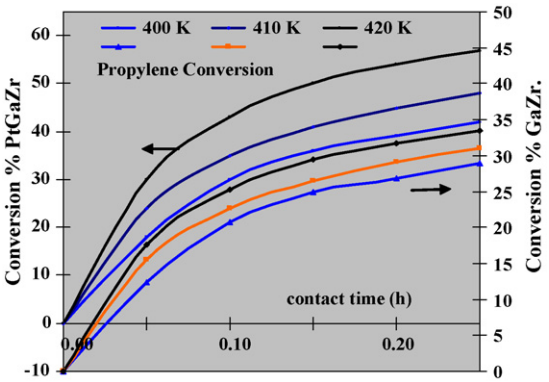

Fig. 4. Conversion of propylene (PtGaZr and GaZr).

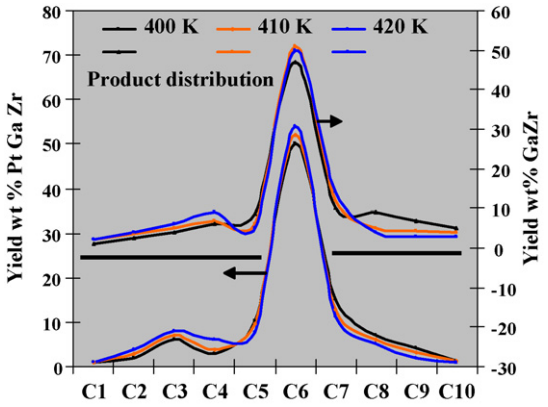

Fig. 5. Product distribution at three temperatures (PtGaZr and GaZr).

conversion of propylene as a function of reaction time and temperature (400, 410 and 420 K, and P_{H2}: 0.9) for both (fresh) catalysts. The figure indicates a relative low sensitivity of the propylene conversion to the reaction temperatures. On those catalysts, the disappearance of propylene follows an apparent rate expression depicted by Eqs. (1) and (2). For the temperature, contact time, stirring speed, and particle diameter used here, the dimerization and the hydrogenation of propylene were not controlled by mass transfer outside of the particle (η_1' and $\eta_2' \sim 1$) for both catalyst and operating conditions other than 420 K. At the latter temperature, the dimerization of propylene seems to be slightly controlled by internal mass transfer of reactant ($\eta_1 \sim 0.9$) for the PtGaZr(F) catalyst. Nevertheless, when the reaction is performed in a slurry type reactor (pilot plant) using a 200 microns catalyst particle an important intraparticle mass transfer control of the reactions was observed. The propylene disappearance as a function of temperature and contact time shown on the right side of Fig. 5 indicated a substantially higher reaction rate for the PtGaZr(F) catalyst than those measured for the GaZr(F) one. The higher activities and a better response to the temperature for the former justify the presence of the noble metal in the catalyst, despite the additional losses of olefins via hydrogenation to propane. The calculated ratio for the propylene dimerization (k_1) and propylene hydrogenation (k_2) reaction using equation 1 and 2 for the two catalyst gives at 400 K and 0.9 MPa P_{H2}

$$\text{dimerization}\,\frac{[\eta_1 k_1]_{\text{PtGaZr}}}{[\eta_1 k_1]_{\text{GaZr}}} = 1.35,$$

$$\text{hydrogenation}\,\frac{[\eta_2 k_2]_{\text{PtGaZr}}}{[\eta_2 k_2]_{\text{GaZr}}} = 1.15$$

These ratios increase with the temperature, indicating a different contribution of the active sites to the reactions. Notice the large difference in dimerization and the small one in hydrogenating capabilities, despite the fact that Pt is recognized as a better hydrogenating metal than the Ga. This phenomenon is due to the presence of benzene that is preferentially adsorbed on very active hydrogenating-dehydrogenating sites. In the absence of propylene (pure benzene 0.4 h contact time, 0.9 MPa P_{H2}, and 400 K) the ratio of benzene hydrogenation reaction constant between the two catalysts is 1.2, showing the additional hydrogenation capabilities of the Pt content catalyst. The adsorption of benzene on this catalyst was verified by the presence of the IR bands at 1968 and 1834 cm^{-1} due to π–proton interactions on PtGaZr(F) surface.

3.6. Activity: effect of hydrogen partial pressure

The propylene conversion is slightly affected (3%) by doubling the hydrogen partial pressure and the aromatic/cycloparaffin ratio is slightly been reduced (4%), as well as the catalyst deactivation. The benzene hydrogenation is increased slightly (5%).

3.7. Selectivity: reaction products

The yield distribution per atom of carbon (wt% on products) is shown in Fig. 5 for both catalysts and the three different temperatures, but a constant space velocity (0.4 h); thus the comparison is made between different propylene conversions. It can be seen that the PtGaZr catalyst results in mainly C_3, C_6, C_7 and C_8 products. The presence of C_4, C_5, C_7, and C_8 is the result of cracking reaction of the initial dimerized products, as shown in Table 1.

The reaction products are divided into three groups of components: aromatics (Ar), cycloparaffins (CP), and paraffins (P). Table 6 shows the distribution of these families in C_5–C_{10} products obtained at the three temperatures, constant residence time and hydrogen partial pressure for PtGaZr catalyst. There is a high selectivity of the catalyst to produce C_6 and C_9 cycloparaffins compounds. The presence of benzene that "saturate" the surface reduces to the minimum the production of aromatics (see Table 6). The test performed with pure benzene at temperatures of 400, 410, 440 K and 0.4 h of contact time showed a small conversion (1.4, 2.3, and 3.3% molar, respectively) into cyclohexane, with no other noteworthy product formed. These conversions were deducted from the values reported in Table 5. Previous studies had shown that by increasing the benzene/propylene ratio beyond 10 (by moles—at the same operating conditions mentioned above) there is no additional effect of benzene in reducing the aromatics and favoring the naphthenes production. Notice the presence of cyclopentane and alkylcyclopentanes intermediaries in the

Table 6
Hydrocarbon families' distribution as a function of temperature (PtGaZr)

Carbon number	C_5	C_6	C_7	C_8	C_9	C_{10}
400 K						
Paraffins	1.9	7	0.9	0.3	0.5	0.1
Aromatic	0	8.3	1.75	0.5	0.4	0.3
Cycloparaffins	9	39	9.8	6.4	3.4	1
410 K						
Paraffins	2.3	8	0.75	0.3	0.5	0.3
Aromatic	0	12.31	2.4	1.3	0.9	0.2
Cycloparaffins	7	37	7.6	4.5	1.8	0.7
420 K						
Paraffins	2.8	7	0.6	0.2	0.4	0.2
Aromatic	0	15.6	3.4	1.8	1.2	0.32
Cycloparaffins	5.8	35.4	6.5	3.2	0.8	0.5

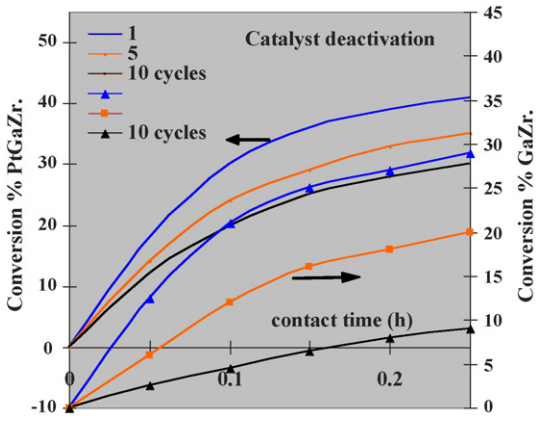

Fig. 6. Catalysts deactivation at 400 K.

products of reaction. The higher the temperature, the higher is the production of C_6 aromatics and the lower the production of $C_{7\text{-}8}$ aromatics, heavy paraffins, and cyclo-paraffins. The detailed analysis of the paraffins indicates that the higher the temperature, the lower the production of $C_{4\text{-}5}$ *iso*-paraffins in comparison with *n*-paraffins. At same level of propylene conversion, the effect of increasing temperatures tends to increase the cracking reaction rate that augments the production of $C_{4\text{-}5}$ *n*-paraffin. The analysis of the C_8, C_9 naphthenes and aromatics indicated that they are mainly mono branched. Increasing the contact time and the level of conversion increases the $C_{7\text{-}8}$ in detriment of C_6 production that could be produced via $C_6 + C_3$ alkylation and cracking is an in-series reaction. The propane is supposed to be formed mainly via hydrogenation of the propylene; nevertheless, it can be also produced via cracking of heavy paraffins formed. Both reaction rates augment with the temperature.

The same analysis performed on the products generated by the GaZr(S) indicated a different behavior. In absence of Pt, the Ga produces a larger proportion of C_6 and C_9 aromatics than naphthenes, as we had reported before [14]. To illustrate the point, we calculated the ratio for C_6 and C_7 between cycloparaffins and aromatics for 400 K and 25% of propylene conversion for both samples. To obtain the same conversion the contact time was 0.2 and 0.55 h (400 K, P_{H2}:8) for the samples with and without Pt. These results show clearly the difference in selectivity of the two catalysts characteristic of the changes on acid site and hydrogen adsorption associated to the Pt

$$\frac{[C_{6CP}/C_{6Ar}]_{PtGaZr}}{[C_{6CP}/C_{6Ar}]_{GaZr}} = 1.6 \quad \text{and} \quad \frac{[C_{7CP}/C_{7Ar}]_{PtGaZr}}{[C_{7CP}/C_{7r}]_{GaZr}} = 1.4$$

3.8. Stability: catalyst deactivation

A decline in activity (Fig. 6) can be observed as a consequence of coke accumulation on the surface (Table 2) enabling a decrease in acidity (Table 4) and metals dispersions (Table 3). The type of carbon can be characterized by the solubility in CS_2 (carboids, insoluble in xylene). The extracted material was 10.5% and 17.4% wt of the coke, respectively with and without Pt on the catalyst. Analysis of the types of compounds present on the spent catalysts by ^{13}C NMR before the extraction with CS_2 shows the characteristic bands at 130, 165 ppm and 5–15 ppm assigned to the naphthenic-aromatics, aromatics, and paraffinic type deposits, respectively. The ratio of the intensities of these signals, calibrated with adamantine were measured for the PtGaZr(S) and GaZr(S) after 10 cycles in continuous operation. This ratio indicated a large difference between the two catalysts. The deposit is more paraffinic in the Pt-content solid due to the presence of high amount of hydrogen in surface (spillover), and to the presence of benzene that occupied the strongest metal and acid sites reducing the transformation of naphthenes into aromatics and polyaromatic. The ratio of the naphthenic-aromatic/paraffinic ^{13}C NMR intensities for the catalyst deactivated at 400 K were 0.5 (PtGaZr(S)) and 0.66 (GaZr(S)) in xylene extracted samples while this ratios were respectively 0.68 and 0.72 on CS_2-extracted catalysts

$$\text{xylene} - \text{extracted}: \frac{[I_{130-150}/I_8]_{PtGaZr}}{[I_{130-150}/I_8]_{GaZr}} = 0.75,$$

$$CS_2 \text{ extracted}: \frac{[I_{165}/I_8]_{PtGaZr}}{[I_{165}/I_8]_{GaZr}} = 0.88$$

The first relative ratio (0.75) showed above is (surprisingly) constant at the temperatures studied here, but those measured on CS_2-insoluble deposit decrease with the increase of temperature due to the important augment in aromatic type of carbon on GaZr sample. In addition the extraction of the carboids reduces the 130 ppm signal (naphthenic) and increases other a 150 ppm (aromatics) that is shifted toward 165 ppm in both spent samples. The analysis of the CS_2-extract by ^1H NMR and IR spectroscopies indicated the presence of some alkyl-diciclo-napthenes, with $C_{5\text{-}6}$ olefinic-rings intercalated by paraffins in a linear polymeric structure (molecular weight between 200 and 400 g) that seems to be the coke precursor. Similar types of compound were found in previous studies on Ga/ZSM-5 [5]. Kiessiling and Froment [29] had determined that the mechanism of Ni SiO_2–Al_2O_3 catalyst deactivation during the dimerization of propylene is due to linear olefins oligomerization on surface. Lagner [30] in 1981 had had

postulated the formation of this cyclooleffinic compound during the dimerization of propylene at temperatures below 500 K on Y zeolite, and Lukyanov et al. [12] had modeled the coke built up for ethene and propylene aromatization on GaHZSM-5 using cycloolefins intermediaries. In our case the presence of a H_2 partial pressure, Pt well dispersed, benzene and low operating temperature limited the aromatization of these adsorbed carboid type material on weak acid sites where it can be hydrocracked. The XPS analysis (Table 4 (FWHM: 3.8 eV) and the ^{1}H NMR (shoulder observed between −20 and +20 ppm due to the proton on the coke with high dipole interaction) confirm that the coke–CS_2 insoluble deposit is less aromatic and poorly defined in Pt containing catalyst. This insoluble material is supposed to be formed early on the strong acid sites (during first and second cycles of operation) in both catalyst, but in the subsequent cycles the carboids are continuously formed and might be converted into lighter products and more coke. On the PtGaZr(S) catalyst, the intermediaries are hydrocracked, and the activity partially preserved, while on GaZr(S) they are transformed into an insoluble carbon deposit. Choudhary et al. [31] reported for the propane aromatization on Ga containing catalyst that the activity and selectivity, as well as the catalyst deactivation were proportional to the total acidity measured –for example – in terms of pyridine chemisorbed. That is not the case for the present catalysts, at the operating conditions used here.

The pyridine adsorption on spent catalyst at 200 and 300 °C shows that the total acidity and L/B ratio are higher for PtGaZr(S) than for GaZr(S) catalyst (compared in Table 5 the values of pyridine adsorbed on fresh and used catalyst that present changes for both L and B sites). Associated with that, the XPS analysis shows different reduction of Ga and Zr dispersion after reaction (see Table 4) on the two catalysts. The changes in metal dispersion are smaller in the PtGaZr(S) than in GaZr(S) catalyst, which explains the survival of more acid sites with differing strengths in the former.

3.9. Deactivation effect on selectivity

In Fig. 6, right side shows the deactivation of PtGaZr catalyst. After having an important initial rate of deactivation (1–5 cycles), later the rate decreased (5–10 cycles). The hypothesis used here is that insoluble coke is initially accumulated on the strongest acid sites, which have minor participation in converting propylene into naphthene. Further on, in spite of formation additional coke intermediaries, the rate of coke accumulation was lower. To support this hypothesis the same test was done at double the hydrogen partial pressure and different temperatures. It was observed that the higher the P_{H2} and the temperature, the lower the deactivation and larger the amount of $C_{3\text{-}6}$ compounds formed, which confirms the idea about the hydrocracking of the intermediaries. The analysis of product distribution shows that catalyst deactivation improves the selectivity toward C_6 naphthenes in detriment of C_6 aromatics production.

Discussion will now focus on the fate of the other catalyst (GaZr(S). It shows an important deactivation after 5 and 10 cycles on stream (Fig. 5, left axis), and the higher the operational temperature, the higher the rate of deactivation. By increasing the hydrogen partial pressure, the rate of deactivation slightly decreased. The product distribution shows that benzene production is favored over that of cyclohexane by catalytic deactivation. The following comparative ratio between the two catalysts after the 1st, 5th and 10th cycle on stream depicts the relative effect of deactivation in selectivity

$$\text{1st cycle}: \frac{[C_{6CP}/C_{6Ar}]_{PtGaZr}}{[C_{6CP}/C_{6Ar}]_{GaZr}} = 1.6;$$

$$\text{5th cycle}: \frac{[C_{6CP}/C_{6Ar}]_{PtGaZr}}{[C_{6CP}/C_{6Ar}]_{GaZr}} = 2.5;$$

$$\text{10th cycle}: \frac{[C_{6CP}/C_{6Ar}]_{PtGaZr}}{[C_{6CP}/C_{6Ar}]_{GaZr}} = 3.5$$

The relative change described above on coked-catalysts shows the lower deactivation of the PtGaZr(S) active site that produces cycloparaffins than those present in GaZr(S), proving the beneficial effect of the Pt presence on stability.

3.10. Mechanism of propylene dimerization

The olefins oligomerization could produce a broad distribution in molecular weight of aromatics, paraffins, and *iso*-paraffins depending on the operating conditions and the catalyst used. In particular propane and butanes can be transformed into aromatics on Ga/Zeolite, following a mechanism that was discussed by Guisnet and Gnep [32], among others and by us [5]; in this case the limiting step seems to be the initial dehydrogenation. For propylene aromatization the reaction can be performed a lower temperature and the reaction rate is controlled by the cycloparaffin intermediary formation and their consecutive dehydrogenation. With PtGaZr(F) catalyst the reaction can be performed even at much lower temperature than with Ga/ZSM-5 or GaZr(F). By using an excess of benzene and a medium hydrogen partial pressure, the reaction rate is controlled only by the cyclization of the naphthenes adsorbed molecules. On the former catalyst, the olefins might be adsorbed in a Ga–O–Si or Ga–O–Zr Bronsted–Lewis dipole acid site where they form a adsorbed carbanion–carbocation, while other is adsorbed in a near by acid sites. The adsorbed species might interact via dipole–dipole and form a larger adsorbed molecule. When this dipole is located in a hexagonal or pentagonal acid sites structure the cycle intermediary could be formed and desorbs to form the cycloparaffins in products. Other olefins located in different on-surface organization might form large linear olefins (C_9–C_{15}) that can be isomerized and desorbed or be cracked and desorbed (a simplified scheme for the path of reactions is shown in Fig. 7). The isomerization and cracking of these adsorbed large molecules produce a series of di and tri branched olefinic intermediaries ($iC_4^=$, $iC_5^=$, $iC_7^=$) and n-$C_{3\text{-}5}$ paraffins. In our case the high selectivity of this catalyst toward cycloparaffins formation indicated that main path of reaction is via cyclo-

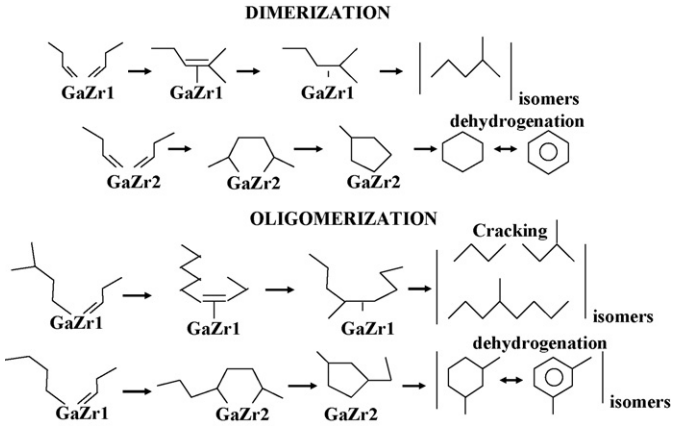

Fig. 7. Scheme (simplified) for the path of reactions.

intermediary formation like was proposed by Kazansky [33]. Isotopic studies performed by Biscardi and Iglesia [34] with ^{13}C propane molecules indicated the presence of some of this intermediaries that we propose here for the olefins dimerization (Table 1). Pt nanocluster might induce a particular organization of the acid site on surface and favor the cycloalkanes production and produces a hydrogen saturation of the surface that limits the aromatization and polymerization to coke.

4. Conclusion

Propylene can be converted into cycloparaffins, and into some paraffins and aromatics by dimerization–oligomerization of propylene on $PtZrGa/SiO_2$ catalyst. Pt and the hydrothermal treatment used to treat a $GaZr/SiO_2$ as-synthesized catalyst generated the following changes in activity, selectivity, and stability:

- promoted the migration of Ga and Zr into the surface;
- increased the total acidity, modified the acid strength distribution, and the Bronsted/Lewis ratio;
- augmented the production of cycloparaffins to their detriment of the paraffins and aromatics;
- modified the amount and the type of carbonaceous deposit formed during the reaction;
- modified the amount of metal exposed and the amount and type of acid sites that survive the deactivation;
- improved the catalyst stability, enhanced by the presence of benzene and hydrogen partial pressure.

Acknowledgments

The authors wish to thank Dr. J. Reverse for the ^{17}Ga NMR analysis, the valuable discussion with Professors J.A. Akerman and J. Kassansky, and the economic support of Simon Bolivar University.

References

[1] T. Xie, K.B. Mc Auley, J.C.C. Hsu, D.W. Bacon, Ind. Eng. Chem. Res. 33 (1994) 449–479.
[2] M. Golombock, J. de Brujin, Ind. Eng. Chem. Res. 39 (2000) 267–271.
[3] Y. Chauvin, S. Einloft, H. Olivier, Ind. Eng. Chem. Res. 34 (1995) 1149–1155.
[4] R. Catani, M. Mandreoli, S. Rossini, A. Vaccari, Catal. Today 75 (2002) 125–131.
[5] R. Galiasso Tailleur, J.B. Platin, Catal. Today 106 (2005) 77–83.
[6] C. Costa, J.M. Lopes, F. Lemos, F. Ramoa, F. Rivero, J. Mol. Catal. A: Chem. 144 (1999) 207–220.
[7] J.L. Bonardet, M.C. Barrage, J. Fraissard, J. Mol. Catal. A: Chem. 96 (1995) 123–143.
[8] L. Johnson, C.H.M. Killian, M. Brookart, J. Am. Chem. Soc. 117 (1995) 6414–6415.
[9] G. Giannetto, R. Monque, R. Galiasso, Tailleur, Catal. Rev. 36 (2) (1994) 271–304.
[10] Z. El Berrichi, L. Cherif, O. Orsen, J. Fraissard, J.P. Tessonier, E. Vanhaecke, B. Louis, M.J. Ledoux, C. Pham Huu, Appl. Catal. A: Gen. 298 (2006) 194–202.
[11] K.J. Chao, P.H. Liu, Catal. Surv. Asia 9 (2005) 11–15.
[12] D. Lukyanov, N.S. Gnep, M.R. Guisnet, Ind. Eng. Chem. Res. 33 (1994) 223–234.
[13] O.V. Bragin, T.V. Vasina, V. Sitnik, N.V. Nekrasov, V.I. Yakerson, Seriya Khimicheskaya 6 (1990) 1250–1257.
[14] J. Park, W. Lee Young, H. Hynun Sik, Korean J. Chem. Eng. 19 (3) (2002) 411–416.
[15] A.L. Propskurin, S.N. Ovcharov, A.Z. Dorogochinsky, O.N. Karatun, Nefttekhimiya 32 (6) (1992) 533–537.
[16] R Galiasso Tailleur, J.B. Platin, US Patent pending (2006).
[17] S. Wu, Y. Han, Y.C. Song, L. Zhao, Y. Di, S.-Z. Liu, F.S. Xiao, Chem. Mater. 16 (2004) 9739–9781.
[18] R. Galiasso Tailleur, Mass transfer in the pores deactivated by Coke, Preprint of the LACTYM congress held in Caracas April (2004).
[19] D. Briggs, M.P. Seah (Eds.), Practical Surface Analysis by Auger and X-ray Spectroscopy, John Wiley, 1987, pp. 511–532.
[20] J.L.Z. Tekie, T.I. Mizan, B.I. Morsi, E.E. Maier, C.P. Sigh, Chem. Eng. Sci. 4 (2004) 549–559.
[21] T. Takeguchi, J.B. Kim, M. Kang, T. Inui, W.T. Cheuh, J. Catal. 175 (1998) 1–6.
[22] C. Cheng, H. He, W. Zou, J. Klinoski, J.A. Goncalvez, L.F. Gladden, J. Phys. Chem. 100 (1996) 390–397.
[23] Y. Diaz, L. Melo, M. Mediavilla, A. Albornoz, J. Brito, J. Mol. Catál. A: Chem. 227 (2005) 7–15.
[24] K. Fang, J. Ren, Y. Sun, J. Mol. Catal. A: Chem. 229 (2005) 51–58.
[25] T. Blasco, A. Corma, M.T. Navarro, J. Perez-Pariente, J. Catal. 156 (1995) 65–74.
[26] O. Gutierrez, G. Fuentes, C. Salcedo, T. Klimova, Catal. Today 116 (2006) 485–497.
[27] A.L. Petre, A. Auroux, P. Gelin, M. Caldararu, N.I. Ionescu, Thermochim. Acta (2001) 177–185.
[28] Z. Gabelica, C. Mayenez, R. Monque, R. Galiasso Tailleur, G. Giannetto, Molecular Sieves, vol. 1, Van Reinhold, NY, 1992, pp. 190–221 (chapter 15).
[29] D. Kiessiling, G.F. Froment, Appl. Catal. 71 (1) (1991) 123–138.
[30] B. Lagner, Ind. Eng. Chem. Process Des. Dev. 20 (1981) 326–331.
[31] V.R. Choudhary, P. Devadas, A.K. Kinage, M. Guisnet, Zeolitas 18 (2/3) (1997) 188–195.
[32] M. Guisnet, N.S. Gnep, Appl. Cat. A: Gen. 146 (1996) 33–34.
[33] V.B. Kazansky, Acc. Chem. Res. 24 (1991), pp. 379–342.
[34] J.A. Biscardi, E. Iglesia, Catal. Today 31 (1996) 207–213.